Spontaneous emission in the optically excited single-electron-tunneling device tuned by the tunneling

Ronghua Li (李荣华), Sen Zhang (张 森), and Weixian Yan (阎维贤)*

College of Physics and Electronics, Shanxi University, Taiyuan 030006, China

**Corresponding author: yanwxsxu@gmail.com*

Received February 25, 2014; accepted July 25, 2014; posted online October 17, 2014

The spontaneous emission spectrum in the optically excited single-electron-tunneling device coupled to the side dot is analytically found to be determined by the 12 exciton-complex optical channels with different optical weight functions. The electronic tunneling channels and optical transition channels co-determine the emission, where the competition between the electron-like and hole-like channels leads to the tail effect and the competition between the lower and higher energy resonant optical channels leads to the blueshift (redshift) of the emission signal.

OCIS codes: 230.5590, 300.2140, 300.0300.

doi: 10.3788/COL201412.112301.

The exciton complexes[1–9] produced by the many-body electron–electron and electron–hole interactions in the single-electron-tunneling (SET) devices[7,10,11], consisting of quantum dots (QDs)[2,7,8,12] with source and drain play vital roles in optical and transport processes[13–19]. Studying the optical processes is an effective way of illuminating the resonance channels generated by the exciton complexes in the optically excited SET. Recently, Zhou *et al.* performed photoluminescence spectroscopy experiment on the coupled QDs systems, where the traces of exciton, charged excitons (exciton X, positively/negatively charged trions $X^{+/-}$, and doubled-charged exciton X^{2-}) had been located in the photoluminescence line shapes[2]. The optical processes in the optically excited QDs with the source and drain was studied by Kuo *et al.* in the framework of Keldysh correlation Green's functions (CGFs)[7], where the exciton, biexciton, positively, and negatively trions were found.

What if we combine these two systems or introduce a second dot into the SET? In this letter, the second externally controlled p-type QD has been introduced as an impurity dot into the optically excited SET, where the two QDs couple to each other via the Coulomb interactions[1–4,7] and their electronic processes are governed by the following Hamiltonian:

$$\begin{aligned} H_{\text{electronic}} &= \sum_{i=(e,h,h_2),\sigma} E_i d^{\dagger}_{i,\sigma} d_{i,\sigma} + \sum_{k,\sigma,l=L,R} \in_k c^{\dagger}_{k,\sigma,l} c_{k,\sigma,l} \\ &\quad + \sum_{k\sigma l} (V_{k,\sigma,l} c^{\dagger}_{k,\sigma,l} d_{e,\sigma} + \text{h.c.}) \\ &\quad + \sum_{i,\sigma}^{(e,h_2,h)} U_{i,i} d^{\dagger}_{i,\sigma} d_{i,\sigma} d^{\dagger}_{i,-\sigma} d_{i,-\sigma} + \sum_{i\neq j,\sigma,\sigma'}^{(e,h)} U_{i,j} d^{\dagger}_{i,\sigma} d_{i,\sigma} d^{\dagger}_{j,\sigma'} d_{j,\sigma'} \\ &\quad + \sum_{i,\sigma,\sigma'}^{(e,h)} U_{i,h_2} d^{\dagger}_{i,\sigma} d_{i,\sigma} d^{\dagger}_{h_2,\sigma'} d_{h_2,\sigma''} \end{aligned}$$

where $d_{i,\sigma'}$ $(d^{\dagger}_{i,\sigma})$ represents the annihilation (creation) electron/hole operator with spin σ in the intrinsic dot; $d_{h_2,\sigma,}$ $(d^{\dagger}_{h_2,\sigma})$ is the annihilation (creation) hole operator with spin σ in the p-type second side dot; $c_{k,\sigma,l}$ $(c^{\dagger}_{k,\sigma,l})$ represents the annihilation (creation) electron operator in source and drain. The first two terms on the right-hand side of Eq. (1) describe the electrons/holes in the two dots and electron reservoirs in the left and right leads, respectively. The third term describes the hopping between the leads and the intrinsic dot. The intra-dot Coulomb interactions in both the intrinsic and side dots are described in the fourth to sixth terms, where the fourth term describes the electron–electron and hole–hole interactions in the two dots, the fifth term describes the electron–hole interactions in the intrinsic dot, and the sixth term describes the electron–hole, and hole–hole interactions between the intrinsic and side dots.

The optical processes can be described briefly as follows: the electrons and holes in the wetting layer are excited by the pumping laser and flow into the intrinsic dot through the relaxation processes[1,3,7,10]. The tunneling rate between the intrinsic dot and two leads is usually much larger than both the electron capture rate from wetting layer to the intrinsic dot and the electron–hole recombination rate within the time scale of the interest. This optical process can be described by the following Hamiltonian:

$$\begin{aligned} H_{\text{optical}} &= \sum_{k\sigma l} (\lambda_0 e^{\text{i}\omega 0 t} b_{e,k,\sigma} b_{h,k,-\sigma} + \text{h.c.}) \\ &\quad + (\lambda_1 e^{\text{i}\omega t} a^{\dagger} d_{e,\sigma} d_{h,-\sigma} + \text{h.c.}), \end{aligned} \tag{2}$$

where $b^{\dagger}_{e(h),k}$ and $b_{e(h),k}$ represent electron (hole) creation and annihilation operator in the wetting laer generated by the pumping laser, and $a^{\dagger}(a)$ is the creation (annihilation) operator for the photon, describing the optical generation and recombination of the electron–hole in the intrinsic dot, with $\lambda_{0,(1)}$ being the coupling strength.

The spontaneous emission spectrum can be calculated by introducing the equal-time CGF $G^{<}_{eh,\sigma}(t,t)$, which represents the optical process of the single-photon emitting via the recombination of the electron in the

conduction band and the heavy hole in the valence band, and is defined as $G^{<}_{eh,\sigma}(t,t) = -\mathrm{i}\left\langle a^{\dagger}(t)d_{h,-\sigma}(t)d_{e,\sigma}(t)\right\rangle$. The equation of motion (EOM) for the CGF $G^{<}_{eh,\sigma}(t,t)$ leads to

$$\left(\omega - E_e - E_h + U_{eh} + \mathrm{i}\frac{\gamma}{2}\right)G^{<}_{eh,\sigma}(\omega) = \lambda_1^{*}F + (U_e - U_{eh})G^{<}_{ehe,\sigma}(\omega) + (U_h - U_{eh})G^{<}_{ehh,\sigma}(\omega) + (U_{hh_2} - U_{eh_2})\left(G^{<}_{ehh_2,\sigma}(\omega) + G^{<}_{ehh_2^{'},\sigma}(\omega)\right), \tag{3}$$

where Fourier transformation to energy space has been employed and the generalized phase-space filling is introduced: $F \equiv \left(\left\langle a^{\dagger}a\right\rangle - \left\langle a^{\dagger}a\right\rangle N_{e,\sigma} - \left\langle a^{\dagger}a\right\rangle n_{h,-\sigma} - n_{h,-\sigma}N_{e,\sigma}\right)$, the averages $\langle ... \rangle$ here are taken over the direct product of photon states and electron–hole states, and the occupation number in the intrinsic dot $N_{e,\sigma} = \left\langle d^{\dagger}_{e,\sigma}d_{e,\sigma}\right\rangle$ is determined by the self-consistent method. The tunneling rate is denoted as $\gamma\,(\equiv \gamma_L + \gamma_R)$ and $(\gamma_{L(R)}$ is the tunneling rate between the intrinsic dot and the left (right) lead). The four CGFs on the right-hand side of Eq. (3) are defined as $G^{<}_{\hat{\Gamma}_{\sigma},\sigma}(t) = -\mathrm{i}\left\langle a^{\dagger}(t)\hat{\Gamma}_{\sigma}(t)d_{h,-\sigma}(t)d_{e,\sigma}(t)\right\rangle$, where the single-particle operators $\hat{\Gamma}_{\sigma}$ represent the intrinsic-dot electron number operator $\hat{d}^{\dagger}_{e,-\sigma}\hat{d}_{e,-\sigma}$, the intrinsic-dot hole number operator $\hat{d}^{\dagger}_{h,\sigma}\hat{d}_{h,\sigma}$, and the number operators of side-dot holes with the opposite spins, $\hat{h}^{\dagger}_{h_2,\sigma}\hat{h}_{h_2,\sigma}$ $\hat{h}^{\dagger}_{h_2,-\sigma}\hat{h}_{h_2,-\sigma}$, describing the four different single-particle screened recombination processes. During the derivation of EOMs of the above four CGFs: $G^{<}_{\hat{\Gamma}_{\sigma},\sigma}(t)$ the following double-particle screened CGFs need to be invoked: $G^{<}_{\hat{\Gamma}^{'}_{\sigma'}\hat{\Gamma}^{''}_{\sigma''}}(t) = -\mathrm{i}\left\langle a^{\dagger}(t)\hat{\Gamma}^{'}_{\sigma'}(t)\hat{\Gamma}^{''}_{\sigma''}(t)d_{h,-\sigma}(t)d_{e,\sigma}(t)\right\rangle$, where double-particle symbol $\hat{\Gamma}^{'}_{\sigma},\hat{\Gamma}^{''}_{\sigma''}$ represents the exciton and two-hole number operators, respectively. These hierarchy structures also include the triple-particle-screened $G^{<}_{\hat{\Gamma}^{'}_{\sigma'}\hat{\Gamma}^{'}_{\sigma''}\hat{\Gamma}^{'''}_{\sigma'''}}(t) = -\mathrm{i}\left\langle \begin{matrix} a^{\dagger}(t)\hat{\Gamma}^{'}_{\sigma'}(t)\hat{\Gamma}^{''}_{\sigma''}(t)\hat{\Gamma}^{'''}_{\sigma'''} \\ d_{h,-\sigma}(t)d_{e,\sigma}(t) \end{matrix}\right\rangle$ and quadruple-particle screened recombination CGFs and consist of 16 EOMs[20].

We solve these equations in real-time domain and then transform them back into frequency space. Fortunately, the analytical result can be obtained through the very lengthy and skillful decomposition techniques:

$$G^{<}_{eh,\sigma}(\omega) = \lambda_1^{*}F\sum_{j=1}^{6}\left(\frac{\zeta_j(1-N_{e,-\sigma})}{\omega - E_g - E^{Xc}_{h,j} + \mathrm{i}\frac{\gamma}{2}} + \frac{\zeta_j N_{e,-\sigma}}{\omega - E_g - E^{Xc}_{e,j} + \mathrm{i}\frac{\gamma}{2}}\right), \tag{4}$$

where $E^{Xc}_{h,j}, E^{Xc}_{e,j}$ are the exciton complexes energies, and ζ_j $(j = 1, 2, ..., 6)$ are the generalized optical weight functions. The resonance energies and the corresponding generalized optical weight functions are found to be

$$\begin{aligned}
&E^{Xc}_{e,1} = U_e - 2U_{eh}; E^{Xc}_{e,2} = U_e + U_h - 3U_{eh};\\
&E^{Xc}_{e,3} = U_e + U_{hh_2} - 2U_{eh} - U_{eh_2};\\
&E^{Xc}_{e,4} = U_e + 2U_{hh_2} - 2(U_{eh} + U_{eh_2});\\
&E^{Xc}_{e,5} = U_e + U_h + U_{hh_2} - (3U_{eh} + U_{eh_2});\\
&E^{Xc}_{e,6} = U_e + U_h + 2U_{hh_2} - (3U_{eh} + 2U_{eh_2});\\
&E^{Xc}_{h,1} = -U_{eh}; E^{Xc}_{h,2} = U_h - 2U_{eh};\\
&E^{Xc}_{h,3} = U_{hh_2} - (U_{eh} + U_{eh_2});\\
&E^{Xc}_{h,4} = 2U_{hh_2} - (2U_{eh_2} + U_{eh});\\
&E^{Xc}_{h,5} = U_h + U_{hh_2} - (U_{eh_2} + 2U_{eh});\\
&E^{Xc}_{h,6} = U_h + 2U_{hh_2} - 2(U_{eh_2} + U_{eh}),
\end{aligned} \tag{5a}$$

$$\begin{aligned}
&\zeta_1 = (1-n_{h_2,\sigma})^2(1-n_{h,\sigma}); \zeta_2 = (1-n_{h_2,\sigma})^2 n_{h,\sigma};\\
&\zeta_3 = (2n_{h_2,\sigma} - 2n^2_{h_2,\sigma})(1-n_{h,\sigma}); \zeta_4 = n^2_{h_2,\sigma}(1-n_{h,\sigma});\\
&\zeta_5 = n_{h,\sigma}(2n_{h_2,\sigma} - 2n^2_{h_2,\sigma}); \zeta_6 = n^2_{h_2,\sigma}n_{h,\sigma},
\end{aligned} \tag{5b}$$

where U_e, U_{eh}, and U_h represent the electron–electron, electron–hole, and hole–hole intra-interaction strengths in the intrinsic dot, respectively, and U_{eh_2} and U_{hh_2} describe the interaction strengths between the holes in the side dot with electrons and holes in the intrinsic dot, respectively.

From the above analytical solution, it can be clearly seen that the correlation functions $G^{<}_{eh,\sigma}(\omega)$ consist of two parts: one part is proportional to $N_{e,-\sigma}$, and the other one proportional to $(1 - N_{e,-\sigma})$. Just like the QD interacting with electron bath in the 2D inversion layer[2,10,14], the introduction of the side dot into the optically excited SET enormously increases the number of the resonance channels, which are shown in Fig. 1. The first two channels from both columns in Fig. 1(b) originally appear in the single-QD case[7], and eight new inter-dot exciton complex channels are generated due to the introduction of the side dot. Besides the enormous increase of the resonance channels, the holes from the second quantum not only participate in the newly added mechanisms but also alter the optical weight functions of the four intra-dot resonance mechanisms, where the static Coulomb interactions between the electrons/holes in the intrinsic dot with holes in the side dot modify the emission spectra both in the number of the signal peaks and linewidth of individual peaks.

The tunneling and optical properties of the optically excited SET are influenced by many parameters, such as dot size, gate, bias voltages, effective mass, confinement potentials, and the compositions of exciton complexes. The eigenvalues $E^{i}_{e,h}$ and eigenfunctions $\psi^{i}_{e,h}$ (x, y, z) of the present work comes from numerical solution of Schrödinger equation by taking the different material parameters (effective mass and energy gaps) for electron and holes in a pyramid InAs/GaAs QD confined in $L = 40$ nm cubic box whose dot height h and base length b are 3.5 and 13 nm, respectively. Then the Hubbard-like interaction parameters among the charge

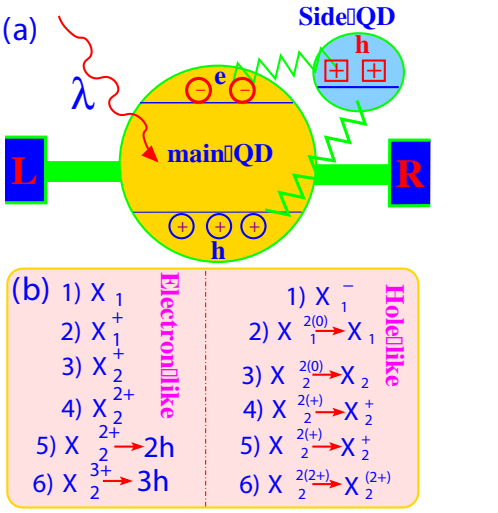

Fig. 1.(a) Schematic view of the optically excited SET, where the symbols ⊕ and ⊖ represent the hole and electron in the intrinsic dot, respectively, ⊞ represents the hole in the side dot, red wavy line stands for exciting lasers, green zigzag lines denote inter-dot electron-hole and hole-hole Coulomb interactions, and L and R represents the left and right leads, respectively. (b) Electron-like (left-hand column) and hole-like (right-hand column) exciton-complexes channels contributing to the spontaneous emission, where $X_i^{n\pm}$ represents neutral ($n = 0$) and charged excitons ($n \neq 0$) and $X_i^{2(n\pm)}$ represents the biexcitons ($n = 0$) and charged biexcitons ($n \neq 0$).

carriers can be obtained from the integral over expectation values of the Coulomb interaction operators[7]. Through these methods, the parameters can be obtained and are presented in Fig. 2, the other parameters are $I = 0.9$, $\Gamma_{h,s} = 0.20$, $R_{eh} = 1.0\times10^{-4}$, and $\gamma_{h,c}N_{h,k} = 0.2$. More accurate parameters can be obtained through the *ab initio*, the first-principle calculations, or extracted and fitted from the experiments[3]. Without loss of generality, the influence of the inter-dot's size can be taken into account by adjusting the electron–hole (U_{eh_2}) and hole–hole (U_{hh_2}) interactions, which capture the essential physics of the inter-dot Coulomb interactions.

The effects of the gate voltage on the weight functions at zero temperature are shown in Figs. 2(a) and (b), where the contour plots of the weight functions $N_{e,-\sigma}\zeta_1$ and $(1 - N_{e,-\sigma})\zeta_1$ have been given. There exists a blue dash critical line, below which the electron-like weight function $N_{e,-\sigma}\zeta_1$ tends to increase with the increase in the gate voltage. Beyond the critical line, the electron-like weight function decreases with the increase in the gate voltage. While the situation is just the opposite for the bias voltage, the electron-like weight function increases with the increase in the gate voltage beyond the blue dash critical line. Both voltages control the weight functions through modulating the electron occupation number in the intrinsic dot, which can be determined self-consistently by invoking the retarded function: $G^r_{e,-\sigma}(t) = -i\theta(t)\left\langle\left\{d_{e,\sigma}(t), d^\dagger_{e,-\sigma}(0)\right\}\right\rangle$. This retarded function together with the other 31 multi-particle retarded functions forms a closed set of hierarchy of EOMs, where 18 resonant electronic tunneling channels can be found[16]. The increase in the bias voltage expands the energy spacing between the left and right chemical potentials, and therefore accommodates more resonance electronic tunneling channels, which undermine the crowding out effect of the tunneling channels due to the excessive increase in the gate voltages. During the process of tuning the electron occupation number by the external voltages, there exists a competition effect between the gate and bias voltages, which indirectly influence the optical processes. The other terms $N_{e,-\sigma}\zeta_i$, $(i = 2, 3,\ldots,6)$ bear the similar evolution profiles as these figures, which are not shown here for saving space.

The electron occupation number in the intrinsic dot versus gate voltage is shown in Fig. 3(a) where the red solid, blue dash, and magenta dash-dotted lines represent the cases of side-dot hole occupancy $n_{h_2,\sigma} = 0.1$, 0.5, and 0.9, respectively. The plateaus in Fig. 3(a) signify the 18 electron–hole complexes-assisted tunneling channels, which are studied in detail in Ref. [15]. The electron occupation number in the intrinsic dot $N_{e,\sigma}$ reaches maximum and then decreases rapidly thereafter. With the increase in the side-dot hole occupancy, this rapid decreasing process occurs at smaller gate voltage and can lead to the tail effect in the spontaneous emission spectra which is described by the modulus of the

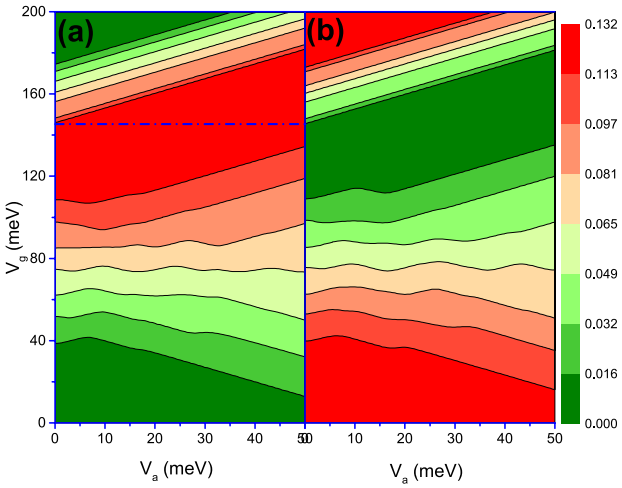

Fig. 2. Contour plots of the weight functions versus gate voltage V_g and bias voltage V_α at zero temperature and half-filling of the side-dot hole number: (a) $N_{e,\sigma}\xi_1$, (b) $(1 - N_{e,\sigma})\,\xi_1$; shows the different behaviors of the electron-like and hole-like weight functions. The parameters used are the biased electron and hole energies: $E^{\text{biased}}_{e(h)} = E^0_{e(h)} + \beta_e V_a - a\,eV_g$, $\alpha = 0.7$, $\beta = 0.5$, and $E^0_e = -140$, $E^0_h = -125$, $U_e = 16.1$, $U_h = 18.5$, $U_{eh} = 16.7$, $U_{eh_2} = 10.0$, $U_{hh_2} = 5.0$ meV. The Fermi level in the electrodes is chosen to be 70 meV below the electron energy level in the intrinsic dot and is assumed to be 60.0 meV above the conduction band minimum. $\gamma_L = \gamma_R = 0.5$, The hole occupation number in the intrinsic dot can be estimated as $n_{h,\sigma} \approx 0.473$.

polarization $P(\omega)$, being proportional to the modulus of CGF: $G^{<}_{eh}(\omega)$. The emission signals versus the gate voltage under the different side-dot hole occupancy are depicted in Figs. 3(b)–(d). The shrinkage of the tails in the emission signal at large voltages can be clearly seen by observing Figs. 3(b)–(d).

The analytical expressions of Eqs. (5a) and (5b) provide a clue on how to control the optical processes through the electronic tunneling processes by tuning both the hole occupation number in the side dot and external voltages. It is clear from Eq. (5b) that ζ_i, $(i = 1, 2,...,6)$ is proportional to $2(n_{h_2,\sigma} - n^2_{h_2,\sigma}), n^2_{h_2,\sigma}, (1 - n_{h_2,\sigma})^2$. If we all the exciton complexes to play roles in the emission spectra, we should choose the side-dot hole occupation number to make the function $f(n_{h_2,\sigma}) = 2(n_{h_2,\sigma} - n^2_{h_2,\sigma}) n^2_{h_2,\sigma}(1 - n_{h_2,\sigma})^2$ take the extreme value. The function $f\ (n_{h_2},{}_{\sigma})$ reaches maximum when $n_{h_2,\sigma} = 0.5$, and the case is depicted in Fig. 3(c) where all 12 exciton complexes optical channels coexist in the contribution to the emission spectra and the emission spectra spread out within the full frequency interval. With the increase in $n_{h_2,\sigma}$ from 0.1 to 0.9, there is a tendency that the speckles in the emission signal move entirely toward the smaller gate voltage direction. This is attributed to the fact that the occupation number $N_{e,\sigma}$ in the intrinsic dot during the electronic tunneling processes rises much more quickly (at smaller gate voltage) with larger side dot hole occupation number, which is self-evident by comparing the three curves in Fig. 3(a).

The emission spectra experience the blueshift[2] when the side-dot hole occupancy is small and redshift when the side-dot hole occupancy is large, which can also be understood through our analytical expression. The ζ_4 and ζ_6 functions are monotonic increasing functions of the side-dot hole occupancy, while the other four ζ_i, $(i = 1, 2, 3, 5)$ are the monotonic decreasing functions when the hole occupation number of side dot is beyond the half-filling. The corresponding resonance energies for the exciton complexes $E^{Xc}_{e(h),4}$ and $E^{Xc}_{e(h),6}$ are the four lowest energies among the all 12 resonance energies, thus resulting in the redshift when the side-dot hole occupation number takes the large value. The situation is just the opposite for ζ_1 and ζ_2 and the corresponding resonance energies $E^{Xc}_{e(h),1}$ and $E^{Xc}_{e(h),2}$ are the four highest energies that lead to the blueshift of the emission signal. Therefore the reasons behind the shifts along the voltage direction and ω — E_g direction are totally different, which cannot be resolved without the analytical solutions of the correlation function $G^{<}_{eh}(\omega)$. The former shift is mainly attributed to the competition between the electron-like and hole-like exciton-complex

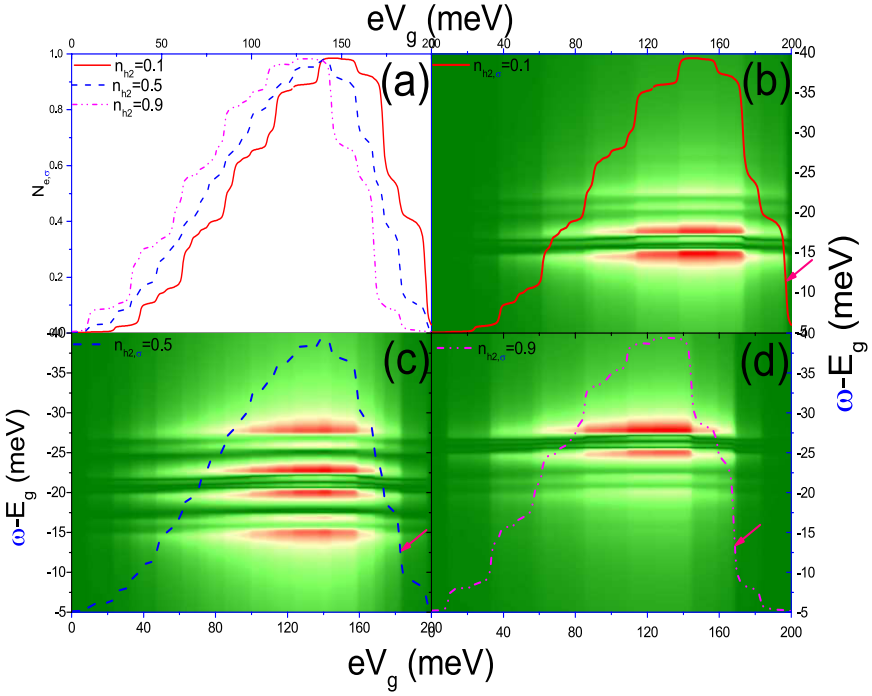

Fig. 3. (a) The occupation number $N_{e,\sigma}$ in the intrinsic dot under the different side-dot hole occupancy $n_{h_2,\sigma}$. Contour-plots of the emission spectra $|P(\omega)|$ versus the gate voltage Vg: (b) $|P(\omega)|$ with the side-dot occupancy $\left\langle \hat{n}_{h_2,\uparrow(\downarrow)} \right\rangle = 0.1$, (c) $|P(\omega)|$ with $\left\langle \hat{n}_{h_2,\uparrow(\downarrow)} \right\rangle = 0.5$; (d) $|P(\omega)|$ with $\left\langle \hat{n}_{h_2,\uparrow(\downarrow)} \right\rangle = 0.9$. The bias voltage is chosen to be $V_\alpha = 20$ meV, and the other parameters are the same as those in Fig. 2. The three arrows indicate the tail effect due to the electron occupancy in the intrinsic dot, where the tail of the emission signals move toward the smaller gate voltage with the increase in the side-dot hole occupancy.

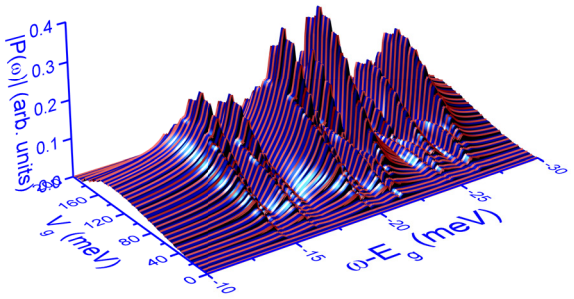

Fig. 4. 3D plots of the emission signal versus the gate voltage, showing the panorama of the spontaneous emission, the parameters used are the same as those in Fig. 3(c), except $\gamma_L = \gamma_R = 0.2$.

optical resonance channels, whereas the latter shift is mainly due to the competition between the different ζ_i functions, where the combined contributions from both the electron-like and hole-like exciton mechanisms work together. In order to give a bird's view of how the electron tunneling influence the optical emission processes at zero temperature, the 3D plot of the spontaneous emission versus the gate voltage is shown in Fig. 4. Along the voltage direction, the plateaus induced by the electron occupation number in the tunneling processes are clearly presented where the peaks along the $\omega - E_g$ are generated by the exciton complexes resonance channels.

In conclusion, we determine the spontaneous emission spectra in the optically excited SET device coupled to the side dot by both the exciton-complex optical channels and electronic tunneling. The optical emission tuned by the electronic processes has been revealed by the numerical and analytical analyses on the external voltages and the side-dot hole occupancy. There exist several competing mechanisms, where the bias voltage is able to postpone the spoiling of the saturation state of the optical weight functions produced by large gate voltages via accommodating more electronic resonance channels. The redshift and blueshift can be realized by altering hole occupation numbers in the side dot. The reason behind these red- and blue-shifts results from the competition between the different optical weight functions with different resonance energies of the exciton complexes. When the lower resonance channels dominate the higher ones, the redshift happens, otherwise, the blueshift appears. The shift also arises with the gate voltages owing to the competition between the electron-like and hole-like exciton optical channels.

This work was supported by the Natural Science Foundation of Shanxi (No. 2008011001-1) and the Shanxi Provincial Foundation for Returned Scholar, and S. Zhang was supported by the Fundamental Fund of Personnel Training (No. J1103210).

References

1. M. A. Dupertuis, K. F. Karlsson, D. Y. Oberli, E. Pelucchi, A. Rudra, P. O. Holtz, and E. Kapon, Phys. Rev. Lett. **107,** 127403 (2011).
2. X. R. Zhou, J. H. Lee, G. J. Salamo, M. Royo, J. I. Climente, and M. F. Doty, Phys. Rev. B **87,** 125309 (2013).
3. M. F. Doty, M. Scheibner, A. S. Bracker, I. V. Ponomarev, T. L. Reinecke, and D. Gammon, Phys. Rev. B **78,** 115316 (2008).
4. I. D. Rukhlenko, M. Yu Leonov, V. K. Turkov, A. P. Litvin, A. S. Baimuratov, A. V. Baranov, and A. V. Fedorov, Opt. Express **20,** 27612 (2012).
5. N. R. S. Kumar, A. J. Peter, and C. W. Lee, Chin. Opt. Lett. **11,** 082501 (2013).
6. M. Royo, J. I. Climente, and J. Planelles, Phys. Rev. B **84,** 235312 (2011).
7. M. T. Kuo and Y. C. Chang, Phys. Rev. B **72,** 085334 (2005).
8. W. X. Yan, W. F. Li, L. P. Xu, J. P. Gong, and T. D. Wen, Phys. Lett. A **374,** 2262 (2010).
9. X. Mi, D. Li, F. Meng, and H. Zhao, Chin. Opt. Lett. **7,** 335 (2008).
10. K. Müller, A. Bechtold, and C. Ruppert, Ann. Phys. **525,** 49 (2013).
11. Y. C. Chang and D. M. T. Kuo, Phys. Rev. B **77,** 245412 (2008).
12. L. Yue, Q. Gong, C. Cao, J. Yan, Y. Wang, R. Cheng, and S. Li, Chin. Opt. Lett. **11,** 061401 (2013).
13. R. C. Ge, S. Weiler, A. Ulhaq, S. M. Ulrich, M. Jetter, P. Michler, and S. Hughes, Opt. Lett. **38,** 1691 (2013).
14. K. S. Virk, D. R. Reichman, and M. S. Hybertsen, Phys. Rev. B **86,** 165322 (2012).
15. W. X. Yan, Y. D. Li, H. R. Wei, L. P. Xu, and T. D. Wen, Phys. E **43**, 1465 (2011).
16. W. X. Yan, Y. P. Zhao, Y. B. Wen, X. P. Li, L. P. Xu, and J. P. Gong, Chin. Phys. B **19,** 027302 (2010).
17. X. P. Li, H. R. Wei, L. P. Xu, and W. X. Yan, Chin. Phys. Lett. **28,** 107306 (2011).
18. J. I. Climente, Solid State Commun. **152,** 825 (2012).
19. R. E. Acosta, A. Zapata, C. A. Duque, and M. E. Mora-Ramos, Phys. E **44,** 1936 (2012).
20. W. X. Yan and R. H. Li, Phys. E **60,** 118 (2014).